Geometrical defects in two-dimensional melting of many-particle Yukawa systems

Arūnas Radzvilavičius*
CoMPLEX, University College London, Gower Street, London WC1E 6BT, United Kingdom
(Received 24 August 2012; published 9 November 2012)

We present a theoretical polygon construction analysis of two-dimensional melting and freezing transitions in many-particle Yukawa systems. Two-dimensional melting transitions can be characterized as proliferation of geometrical defects—nontriangular polygons, obtained by removing unusually long bonds in the triangulation of particle positions. A liquid state is characterized by the temperature-independent number of quadrilaterals and linearly increasing number of pentagons. We analyze specific types of vertices, classified by the type and distribution of polygons surrounding them, and determine temperature dependencies of their concentrations. Solid-liquid phase transitions are followed by the peaks in the abundances of certain types of vertices.

DOI: 10.1103/PhysRevE.86.051111 PACS number(s): 64.60.Cn, 52.27.Lw, 61.20.−p

I. INTRODUCTION

For a few decades, melting and freezing transitions in two-dimensional many-particle systems have been investigated in a variety of experimental and computational studies, without reaching a definite conclusion regarding its nature. According to the most widely accepted Kosterlitz-Thouless-Halperin-Nelson-Young (KTHNY) theory, melting of a single two-dimensional (2D) crystal occurs via two continuous phase transitions, first from a solid to hexatic phase and then from the hexatic to an isotropic fluid [1,2]. The theory also predicts proliferation of unbound topological defects—dislocations and then free disclinations—which play a crucial role in 2D phase transitions and break positional and orientational order. Some experiments and theoretical studies, however, suggest a first-order grain-boundary-induced melting scenario in polycrystalline systems [3,4].

Although in two dimensions a true crystalline order cannot survive at finite temperatures $kT > 0$ [5,6], a quasi-long-range translational order is observed at the conditions of strong coupling, for example, in complex plasma layers [7] or charged colloidal suspensions [8]. Over the years, a broad range of empirical criteria was developed to accurately determine melting and crystallization points [9]. Perhaps one of the most famous examples is the Lindemann criterion, which has been applied extensively in three-dimensional melting and freezing, while its generalized version has been used in some studies of two-dimensional transitions [10]. Other methods frequently make use of topological defect fractions, bond orientational order parameters, orientational and positional correlation functions, as well as Einstein frequencies [11]. In a recent work, a polygon construction method by Glaser and Clark [12–14] was employed to characterize transitions in a rapidly heated and cooled two-dimensional complex plasma experiment [15].

Systems of strongly correlated particles in complex plasmas are of particularly high importance in the experimental studies of phase transitions. Complex plasma usually consists of polymer microparticles immersed in a weakly ionized gas, where distinct dust grains are known to interact through the Yukawa (Debye-Hückel) interaction [16]. Convenient time and length scales of these systems allow for the direct optical observation of collective many-particle phenomena as well as accurate measurements of individual particle positions by the means of video microscopy [17–19].

In a recent experiment, the phenomenon of superheating was observed in a solid state of two-dimensional complex plasma [20]. It was demonstrated that, during a rapid heating process, the concentration of defects can stay low and complex plasma can retain the properties of a solid even at the temperatures above a melting point. The same experimental results were later analyzed by the method of geometrical defects [15], originally developed by Glaser and Clark, which we use in the current work.

Geometrical defects in a polygon construction method are identified by removing unusually long bonds in the triangulation map of particle positions, so that resulting polygons have three or more sides. It was shown that this method provides great sensitivity and unveils some interesting features, undetectable by the conventional analysis of topological defects [15]. As another measure of disorder, the abundance of different kinds of vertices, grouped according to the type and order of the adjacent polygons, was suggested in the same work. Unexpected spikes in the time dependencies of vertex fractions were reported; however, the nature of these peaks remained unclear.

This paper reports on numerical studies of two-dimensional melting and crystallization in strongly coupled Yukawa systems. Langevin dynamics simulations are performed to simulate gradual heating and cooling. Melting and crystallization points are determined employing orientational order parameters and topological defect fractions. However, the main motivation behind the current work is to present the method of geometrical defects and vertex fractions in the polygon construction as a sensitive tool to analyze the order-disorder transitions and characterize the state of a two-dimensional system. Furthermore, our findings resolve the issue of the prominent peaks in the temperature-dependencies of certain types of vertex concentrations [15], by showing that peaks correspond to the initial and final stages of the order-disorder phase transition.

In the following section, we briefly describe the model system and simulation methods as well as essential tools used in the analysis of phase transitions. Main results of the

*a.radzvilavicius.12@ucl.ac.uk

simulations and numerical analysis are presented in Sec. III, while Sec. IV summarizes the article.

II. SIMULATION

A. Model system

A widely used approximation to describe interactions between particles in complex plasmas is the Yukawa interparticle potential energy [16]:

$$V_{ij} = Q^2(4\pi\varepsilon_0 r_{ij})^{-1}\exp(-r_{ij}/\lambda_{\mathrm{D}}). \tag{1}$$

Here, Q is the charge of a particle, r_{ij} is the distance between particles i and j, λ_{D} stands for the Debye length, which accounts for the screening of the interaction by other plasma species.

Strongly coupled many-particle systems with Yukawa interactions are fully characterized by two dimensionless parameters, namely the coupling strength $\Gamma = Q^2/(4\pi\varepsilon_0 b k_{\mathrm{B}} T)$ and screening parameter $\kappa = b/\lambda_{\mathrm{D}}$, where b is the two-dimensional Wigner-Seitz radius [21]. In the simulations presented here we set the screening strength to the constant value of $\kappa = 2$, which is close to the values achievable in complex plasma experiments [20,22]. Nevertheless, the method of geometrical defects and vertex fractions could be applied to the systems with different values of screening strength, as well as other types of interparticle potentials.

As a scale of length in our numerical simulations, it is convenient to choose the Wigner-Seitz radius b, which is directly related to the areal number concentration of particles, $n = 1/(\pi b^2)$. Therefore, the corresponding scale of energy is $\epsilon = Q^2/(4\pi\varepsilon_0 b)$ and time is scaled according to the value of an inverse plasma frequency:

$$\omega_0^{-1} = \left(\frac{Q^2}{4\pi\varepsilon_0 m b^3}\right)^{-1/2}. \tag{2}$$

The model system consists of $N = 2430$ identical particles in a rectangular simulation box of area 85.71×89.07, interacting via the Yukawa potential. Periodic boundary conditions are applied and, since the interparticle potential is short-ranged, the cutoff distance is set to $r_{\mathrm{c}} = 8$. Only particle pairs separated by less than r_{c} are taken into account in the force calculation.

We study order-disorder transitions in the model system by performing Langevin dynamics simulations with slow changes of temperature. Particle positions are updated according to the dimensionless Langevin equation

$$\ddot{\mathbf{r}}_i = -\boldsymbol{\nabla}_i V(\mathbf{r}_1,\ldots,\mathbf{r}_N) - \mu\dot{\mathbf{r}}_i + \mathbf{f}_i, \tag{3}$$

where $\mathbf{f}_i$ represents a randomly fluctuating Brownian force. In a thermodynamic equilibrium $\langle \mathbf{f}_i(t)\rangle = 0$, while the friction coefficient μ is related to the Gaussian noise $\mathbf{f}_i(t)$ by the fluctuation-dissipation theorem [23]

$$\langle \mathrm{f}_i(t)\mathrm{f}_j(t')\rangle = 2\mu k T_{\mathrm{ref}}\delta_{ij}\delta(t-t'), \tag{4}$$

where $i, j \in \{1,\ldots,N\}$ and kT_{ref} is the desired target temperature in the units of ϵ. In our simulations we use $\mu = 0.2$. The Langevin equation is integrated numerically employing an impulse method of integration [24].

B. Analysis

A common way of analyzing the structure of a two-dimensional many-particle system is calculation of a Delaunay triangulation, which yields a network of bonds connecting each particle with its nearest neighbors. A coordination number can be assigned to each particle, which is a number of the triangulation bonds between the particle and its closest neighbors. The coordination number of a particle in a perfect hexagonal lattice is always equal to six. Topological defects are identified as particles with a different coordination number, usually five or seven.

Two most common defect types are the disclination (a single particle with a non-sixfold coordination) and the dislocation (two connected particles with five and seven closest neighbors) [25]. Quite frequently, defects organize themselves in lengthy chains or grain boundaries, indicating a polycrystalline structure of the system. As an alternative, a Voronoi construction is sometimes used in the context of dusty plasmas, where defects are identified as non-six-sided polygons [3,26–28].

To quantify the abundance of topological defects, we use the defect fraction (DF), which is defined as a number of vertices with a coordination number other than six, normalized to the total number of particles N [28].

The polygon construction is a different way of characterizing defects in 2D systems [12,13,15] and helps to identify empty volumes in two-dimensional liquids [29]. The authors of Ref. [12] analyzed bond-angle and bond-length probability distributions in dense 2D liquids. It was shown that disordered regions of a liquid exhibit multiple peaks in a bond-angle probability distribution, with extra peaks corresponding to the square lattice. At the same time, triangularly oriented clusters had a single peak and well-expressed triangular order. The structure of a two-dimensional system, therefore, was described as a square-triangular tiling containing numerous tiling faults.

A triangle, which is the only kind of polygon in the initial triangulation of particle positions, is considered as a nondefective entity. To identify geometrical defects, certain bonds are removed from the triangulation map, so that two polygons sharing a common bond are merged into one. Two possible approaches for the selection of bonds were suggested: either use a bond-length threshold or identify a bond that is opposite to the unusually large angle between a pair of adjoining bonds. In our analysis we follow the authors of Refs. [12,15] and use the critical bond angle of $\alpha = 75^\circ$.

The construction of a polygon map is illustrated in Fig. 1. Figure 1(a) shows the triangulation map of particle positions, where most of the particles are connected with six closest neighbors. Some vertices, however, have five or seven bonds and are marked by small triangles and squares. These particles are considered as topological defects and are all part of a lengthy grain boundary. Triangulation bonds marked by bold lines are facing bond angles larger than the critical value of $\alpha = 75^\circ$ and, therefore, are selected for removal. The resultant polygon map is presented in Fig. 1(b). Geometrical defects

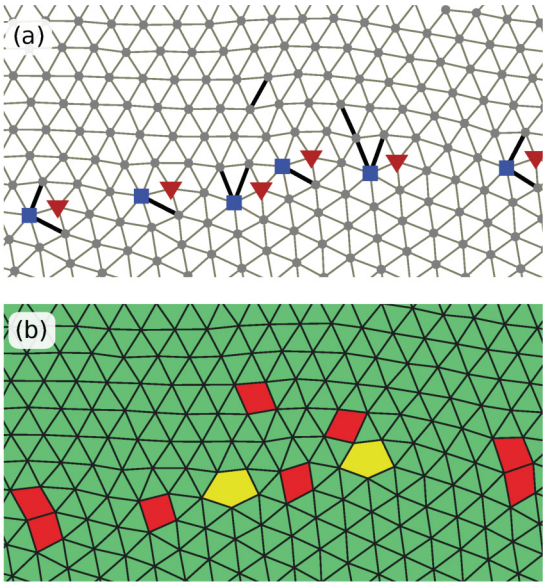

FIG. 1. (Color online) Triangulation map of a polycrystalline Yukawa solid, with topological defects marked as squares and triangles (a). By removing the bonds facing unusually large angles (marked by bold lines), the polygon construction (b) is obtained. In general there is no one-to-one correspondence between topological and geometrical defects.

are identified as nontriangular polygons, that is, quadrilaterals and pentagons. Although the defects appear in a close vicinity of the grain boundary, there is no one-to-one correspondence between the polygons and topological defects.

The polygon construction contains geometrical information about bond lengths and angles, as well as topological information about the nearest-neighbor connections. The method has also the advantage of providing a gradation in the severity of geometrical defects. Quadrilaterals are the least severe, while pentagons and hexagons are more severe and indicate large excess volumes. Topological defects, on the other hand, provide only a binary measure of local orientational disorder, that is, at the specific location of a vertex, there either is a defect or there is not.

The gradation of defects in the polygon method allows for a greater sensitivity identifying and classifying disorder [15]. To characterize the state of our model system and the abundance of geometrical defects, we use four distinct order parameters $P_n = N_n/(2N)$ $(n = 3, 4, 5, 6)$, defined as the number of polygons with n sides N_n, normalized to the doubled number of particles $2N$.

Figure 2 provides a classification scheme for vertices, according to the configuration of polygons arranged around them. The abundance of different vertex types serves as another way to characterize disorder and identify the manner in which polygons cluster together. In a perfect crystal, one would observe only vertices of type A. In a regular square-triangular tiling, only vertices of types A–D are allowed [12]. Types J and K correspond to the topological disclinations, while a vertex L features a severe pentagonal defect. To quantify the abundance of different vertex types, we calculate fractions X_Y, defined as the number of vertices of a certain type Y normalized to the total number of particles in the polygon construction.

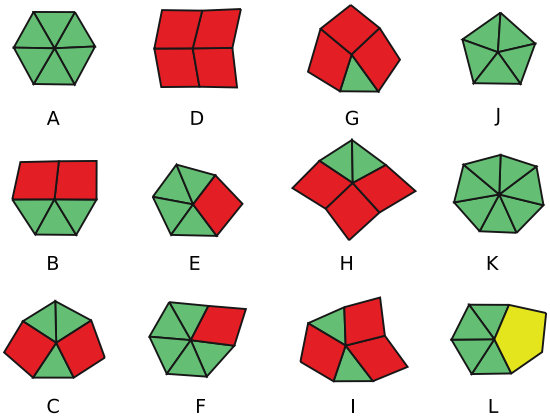

FIG. 2. (Color online) Twelve types of vertices, frequently observed in the polygon construction of two-dimensional Yukawa systems. Vertices are classified by the number and relative distribution of polygons around a vertex.

Unexpected spikes in the time dependencies of parameters X_E and X_F were detected in the analysis of the recent super-heating experiment [15], suggesting that some of the vertices might be metastable or exist only in a narrow range of temperatures. One of the goals of our work is to resolve this issue.

Phase transitions in two-dimensional systems are usually identified by the sudden change in orientational or translational order parameters. The local orientational order parameter for a particle j is defined as [30]

$$\psi_{6j} = \frac{1}{N_j}\sum_{k=1}^{N_j}\exp(6i\theta_{jk}), \tag{5}$$

where θ_{jk} is the angle between the bond connecting particles j and k and some fixed direction. N_j is the coordination number of the particle j. The magnitude $|\psi_{6j}|$ is close to unity for a particle inside a hexagonal lattice but is small close to the domain walls (grain boundaries) or in a liquid. On the other hand, the value of a complex argument $\arg(\psi_{6j})$ represents the angular orientation of a neighborhood or entire domain.

The parameter $\psi_6 = |\langle\psi_{6j}\rangle|$, that is, a magnitude of the averaged complex orientational order parameter, defines the overall orientational order of the system. In polycrystalline solids, however, complex numbers ψ_{6j} corresponding to the particles from different domains tend to cancel in the averaging process. Therefore, ψ_6 approaches very small values in the limit of an infinite sample size. Another parameter can be used in such cases, namely $\psi_{|6|} = \langle|\psi_{6j}|\rangle$, which represents the average local orientational order of the whole system [9].

III. RESULTS

We start our simulations with a defect-free lattice in a strongly coupled state and the temperature of $kT = 10^{-7}$. The system is then heated over the period of time of $\Delta t = 240\,000$, until the temperature of $kT = 0.005$ is reached. The stage of steady cooling then follows, restoring the temperature to its initial value [see, for example, Fig. 8(e)]. The chosen rate of heating is low enough to reach the equilibrium at each step

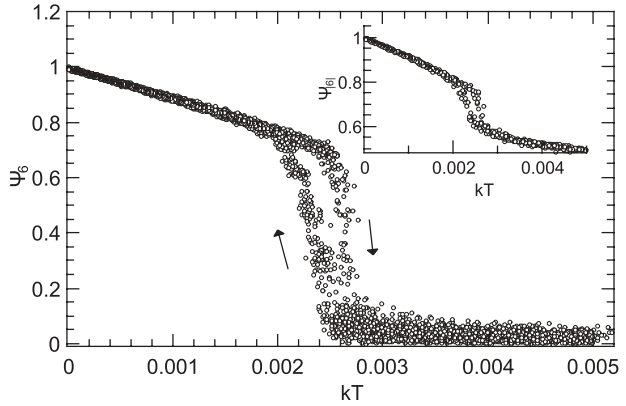

FIG. 3. Averaged orientational order parameters ψ_6 and $\psi_{|6|}$ of a 2D Yukawa system during the heating and cooling simulation cycle.

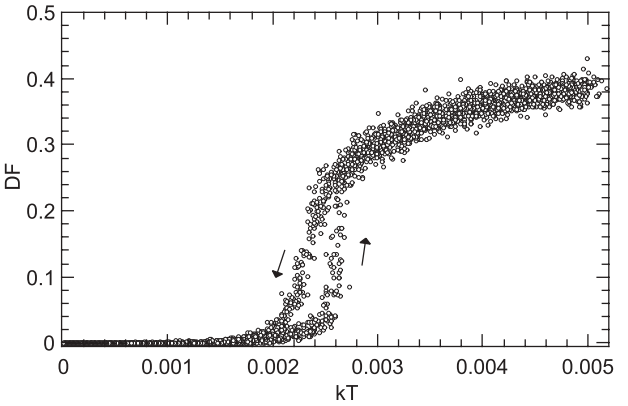

FIG. 4. Topological DF as a function of the kinetic temperature kT.

of the simulation outside the region of a fast order-disorder transition. Therefore, lower rates of heating and cooling would not substantially change the qualitative results of our numerical experiments, except in the close vicinity of the transition, which we discuss later.

The peak temperature is chosen to be well above the melting point, as found by previous studies [11,31]. The actual kinetic temperature of the system is calculated from observed particle velocities, $kT = \langle v_i^2 \rangle/2$, and is found to fluctuate around the prescribed values of $kT_{\rm ref}$, with the fluctuations being proportional to the temperature. We keep track of the order parameters and defect fractions throughout the whole cycle. In this section, we first investigate the orientational order of the 2D system and then turn to the defects and polygons.

Initial values of both orientational order parameters ψ_6 and $\psi_{|6|}$ are very close to unity, as Fig. 3 shows, and correspond to the defect-free hexagonal lattice. The system exhibits a sudden loss of orientational order in the temperature range of $kT = 0.0025$–0.0027 (the corresponding coupling parameter values are $\Gamma = 370$–400), which is the signature of a melting phase transition. Our observations are in fair agreement with Refs. [11,31], where phase transitions in two similar 2D systems were observed near the values of $\Gamma = 384$ and $\Gamma = 415$. At the end of the heating phase, ψ_6 drops below 0.1 and $\psi_{|6|}$ drops to the value of approximately 0.5.

As the temperature is gradually lowered, a 2D Yukawa liquid freezes back to the hexagonal lattice. However, the evolution of the order parameters does not follow exactly the same path as observed in the case of melting and hysteresis (Fig. 3). ψ_6 stays low until the temperature of $kT = 0.0024$ is reached, which is lower than the melting point. Changes in $\psi_{|6|}$ also occur at somewhat lower temperatures and are not as abrupt as in the case of melting. As we show later, the effect of hysteresis is most likely a result of the finite rate of heating and cooling.

The concentration of topological defects during the stage of slow heating exhibits a similar trend, with a weak temperature dependence before and after the transition; see Fig. 4. A sudden proliferation of defects is observed in the range of $kT \approx 0.0025$–0.0027. Changes in the defect concentration during the gradual cooling are not as abrupt and occur at somewhat lower temperatures, $kT \approx 0.0024$–0.0022.

Four typical snapshots of particle positions during the transition are shown in Fig. 5. Here triangles correspond to the particles with only five nearest neighbors, while squares mark positions of vertices with seven triangulation bonds. In a solid phase [(Fig. 5(a)], defects mostly appear as quartets, composed of two disclinations with five bonds and two vertices with seven neighbors. Alternatively, this four-defect complex can be treated as a bound pair of two dislocations. Apparently, this kind of topological fault does not significantly change either positional or orientational order. Larger defect complexes, consisting of more than four defective vertices, emerge before the melting transition.

As is illustrated in Fig. 5(b), during the melting transition (e.g., $kT = 0.0026$) defect complexes grow and spread. However, as can be seen in Fig. 5(b), large defect-free patches still exist, suggesting that the transition from a defect-free lattice to

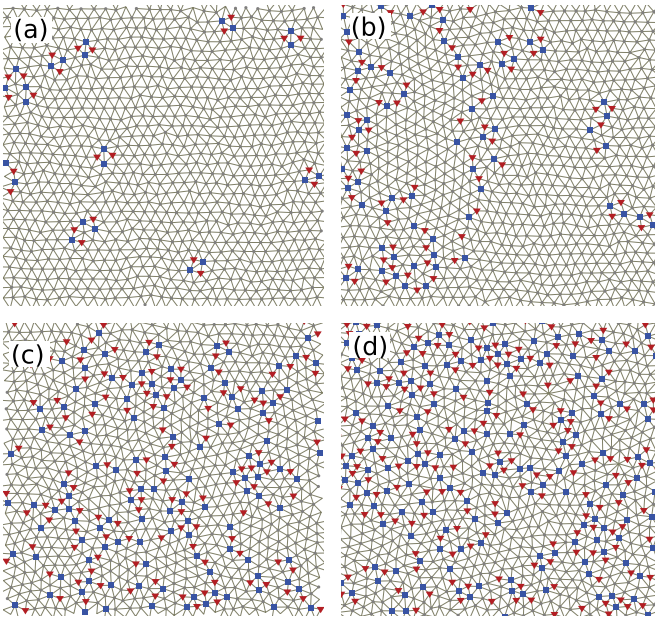

FIG. 5. (Color online) Typical arrangements of topological defects during the melting transition of a 2D Yukawa system. Triangles here represent particles with five closest neighbors, while squares mark vertices with the coordination number equal to seven. The corresponding temperatures are $kT = 0.00245$ (a), 0.0026 (b), 0.0027 (c), and 0.0045 (d).

the disordered state is not homogeneous. Bound dislocations are still found in the ordered patches, however, are seldom seen. While some disclinations and dislocations are present, they are clearly not the main cause of the loss of order; most of these defects appear as parts of larger regions of condensed defect groups and chains. This observation supports the theory of grain-boundary-induced melting [3,4,34], or possibly the coexistence of hexatic and liquid states, as described in Ref. [35]. Further investigations of larger systems would be needed to unambiguously determine the mechanism of the melting transition.

Finally, at the end of the transition [Fig. 5(c)], topological defects form large interconnected complexes, destroying orientational order completely. Free dislocations and disclinations can still be occasionally found in the larger groups of defects. The distribution of defects becomes homogeneous in a high-temperature liquid [Fig. 5(d)].

As the system is slowly cooled, defect complexes and large defect-free regions can still be found at temperatures as low as $kT = 0.0022$, together with some free dislocations. At lower temperatures, however, these complexes tend to shrink and rearrange, eventually leaving only bound and free dislocations as well as interstitial particles. The final configuration corresponds to the nearly perfect triangular lattice with a few free dislocations, leading to the low defect concentration and values of the orientational order parameter close to unity.

Previous studies of similar systems [32] suggest that the effect of hysteresis might be caused by the finite rate of heating and cooling. We test this hypothesis by analyzing the evolution of topological defect fraction at the fixed prescribed temperature of $kT_{\mathrm{ref}} = 0.002\,43$, starting from either liquid or solid initial state. According to Fig. 6, at this temperature the system slowly switches between high and low values of the order parameter, corresponding to the defect configurations depicted in Figs. 5(a) and 5(c). Therefore, there is a range of temperatures in which ordered and disordered states are unstable and have approximately the same probabilities to be observed, as reported in Refs. [32,33]. No hysteresis should occur in the limit of infinite simulation time.

Let us now turn to the analysis of the polygon construction. The initial defect-free lattice corresponds to a triangular tiling. Therefore, the triangle is the only type of polygon present in the

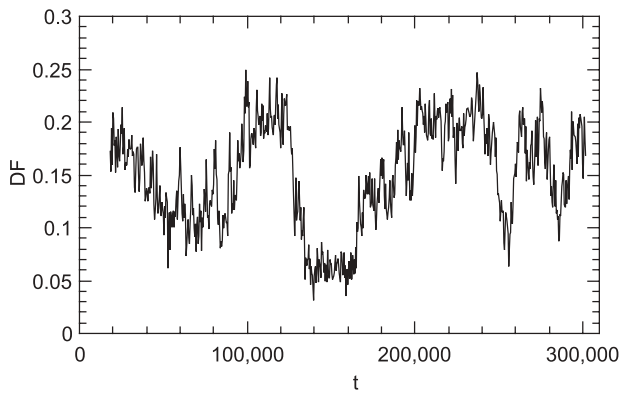

FIG. 6. Time series for the topological DF at the prescribed temperature of $kT_{\mathrm{ref}} = 0.002\,43$.

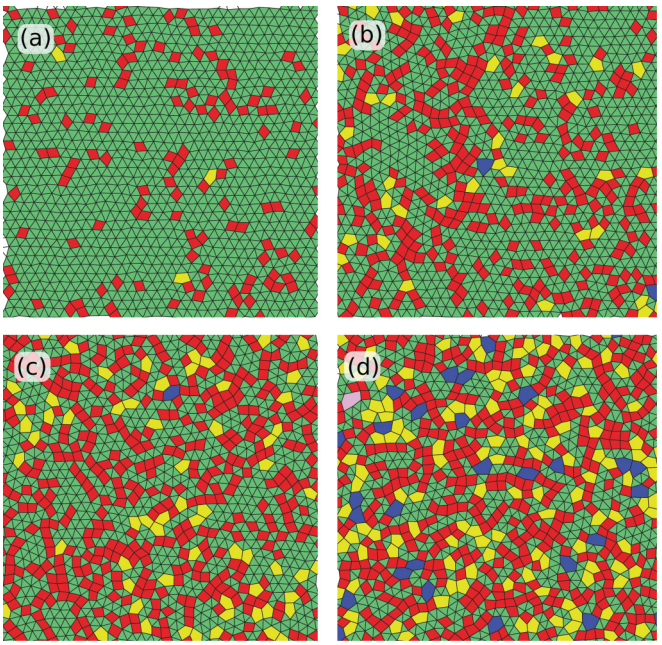

FIG. 7. (Color online) Typical arrangements of geometrical defects during the gradual heating stage in a 2D Yukawa system: solid phase at $t = 45\,002$ (a), configurations during (b) and right after (c), the solid-liquid transition and high-temperature liquid phase at $t = 120\,000$ (d). The corresponding temperatures are $kT = 0.0018$ (a), 0.0026 (b), 0.0027 (c), and 0.0045 (d).

original configuration. As the system is continuously heated, quadrilaterals and occasional pentagons appear. As can be seen in Fig. 7, quadrilateral defects tend to cluster together, forming long chains or "ladders" in a solid phase [Fig. 7(a)] or larger patches of a distorted square lattice in a liquid [Fig. 7(c)]. Defect-free zones are still present during the initial stage of solid-liquid transition, e.g., at the temperature of $kT = 0.0026$, as depicted in Fig. 7(b). Solitary hexagons appear much later and are most abundant in the high-temperature Yukawa liquid [Fig. 7(d)].

The quadrilateral is a first type of geometrical defect to appear in a low-temperature solid, first seen near the temperature of $kT = 5 \times 10^{-4}$. This is as expected, since the quadrilateral is the least severe geometrical defect. Also, it is the most abundant type of defect in both solid and liquid states. The parameter P_4, defined as a number of quadrilateral defects normalized to $2N$, increases steadily as the temperature rises during early stages of heating. As is demonstrated in Fig. 8(b), the proliferation rate gets significantly higher as the temperature reaches the value of $kT = 0.0025$ and the melting transition begins. The rapid transition ends at around $kT = 0.0027$, where the order parameter fluctuates around the value of $P_4 = 0.20$.

The abundance of quadrilateral defects in the two-dimensional Yukawa liquid does not change significantly as the temperature is further increased. Therefore, we suggest that a 2D liquid right after the phase transition can be characterized by the temperature-independent value of the quadrilateral order parameter close to $P_4 = 0.20 \pm 0.01$. These observations are illustrated in Fig. 8 as time series for the order parameter [Fig. 8(b)] and temperature kT [Fig. 8(e)].

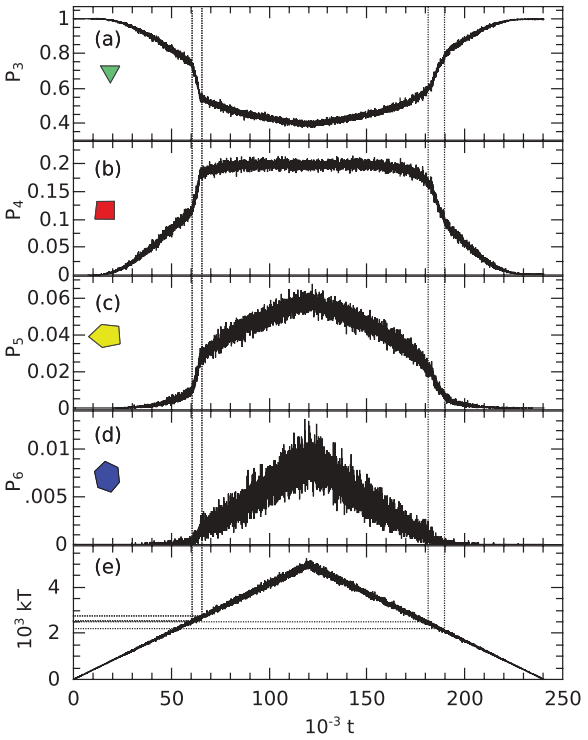

FIG. 8. (Color online) Time series for order parameters P_3 (a), P_4 (b), P_5 (c), and P_6 (d), characterizing the abundances of triangles, quadrilaterals, pentagons, and hexagons in the polygon construction of the 2D Yukawa system. Time series of the kinetic temperature kT is presented in panel (e). Vertical lines mark the beginning and ending points of the melting transition as well as corresponding points during the crystallization.

Occasional pentagonal defects are first spotted at the temperature of nearly $kT = 0.001$. The most significant proliferation of these defects takes place in the range of $kT = 0.0025$–0.0027, where the value of a pentagonal order parameter changes from $P_5 = 0.01$ to $P_5 = 0.03$. After the melting transition, P_5 increases almost linearly with the temperature, at a constant rate. We may conclude that in the context of pentagonal defects, the liquid state can be characterized by values of the order parameter $P_5 > 0.03$ and a steady growth in a number of pentagons.

In our simulations, we observe only a relatively small number of hexagonal defects, with the highest value of an order parameter close to $P_6 \approx 0.012$. Although the time and temperature dependencies of P_6 are rather noisy [see Fig. 8(d)], some general observations can still be made. The most noticeable spread of hexagons starts at about $kT = 0.0025$, which roughly coincides with the start of the melting transition. Afterwards, P_6 seems to increase steadily.

Geometrical defects arrange themselves around the particles in a variety of ways. Some of the most frequent are classified in Fig. 2 as vertex types A to L [12,15]. In a perfect triangular lattice, one would observe only the type A, where six triangles join forming a hexagon. In a liquid, where quadrilaterals tend to form interconnected complexes and "ladders" (Fig. 7), the number of vertices B, D, G, and H is expected to increase.

As we can see, the arrangement of polygons with respect to a certain vertex can be used as an indicator of disorder throughout melting and freezing transitions. Therefore, we further investigate the evolution of vertex fractions $X_Y = N_Y/N$, defined as the ratio of a number of vertices for a certain vertex type N_Y to the total number of particles N.

Vertices E and F are the first to appear when the defect-free system is slowly heated. This observation suggests that there is no tendency for the quadrilaterals to cluster together during the initial stages of heating. Just as the quadrilateral defects, these vertices are first observed at the temperature of $kT \approx 5 \times 10^{-4}$. Both vertex types E and F contain a single quadrilateral—the least severe geometrical defect—and four or five triangles and are created by removing an inner (E) or outer (F) bond from a vertex type A. Therefore, the abundances of vertices E and F have essentially identical time and temperature dependencies (third panel of Fig. 9).

As the temperature rises, the order parameter X_E grows until the critical value of $kT \approx 0.0025$ and the fraction of $X_E \approx 0.175$ is reached. As a matter of fact, it is approximately the same temperature that marks the start of the rapid melting transition, i.e., the sudden loss of orientational order, the rapid growth in a number of topological defects, squares, and pentagons. As geometrical defects proliferate further at higher temperatures, the number of vertices E and F monotonically diminishes.

Vertex types B and C both contain two quadrilaterals and three triangles but differ in the order they are arranged around a

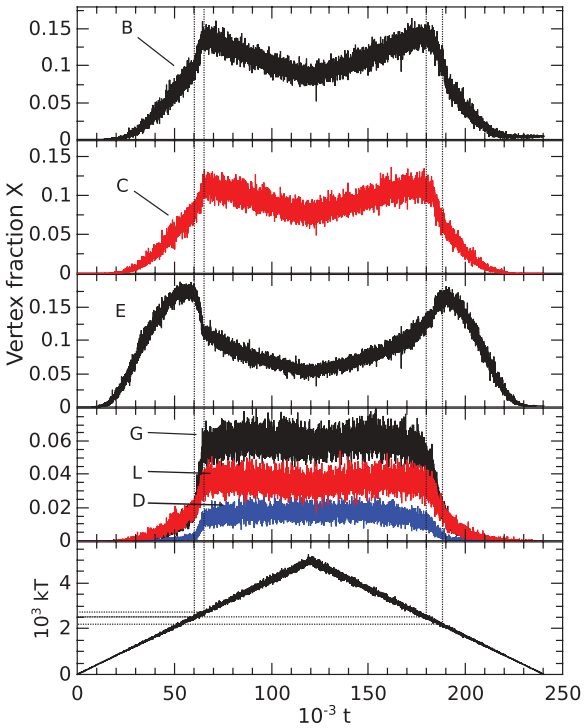

FIG. 9. (Color online) Time series for vertex fractions and the temperature kT. The time dependence of a vertex fraction X_F is virtually identical to the one for vertex E and therefore is not shown here. Vertical lines mark the beginning and ending points of the rapid order-disorder transition and similarly peak positions during the crystallization.

vertex. Two quadrilaterals of a vertex type B share a common edge (Fig. 2), while in a vertex C they are separated by a triangle or two. Vertex concentrations X_B and X_C depart from zero significantly around $kT = 0.001$ and grow further with the kinetic temperature. The order parameter X_B reaches its highest value of 0.14 at the temperature of $kT \approx 0.0027$, which coincides with the final transition to the liquid phase (Fig. 9). Approximately the same is true for the vertex fraction of the type C, which reaches its highest value $X_C \approx 0.12$ close to the temperature of $kT \approx 0.0027$. As the 2D liquid is heated further, the concentrations of vertices B and C decreases.

Vertex fractions for types D, G, H, L, and I all share similar time and temperature dependencies (see the fourth panel of Fig. 9 for the fractions of types D, G, and L; time dependencies of parameters X_I and X_H are nearly identical to the one for the type L and are therefore not shown in the figure). They all feature a steady growth before the temperature of $kT = 0.0025$ is reached, rapid change throughout the melting transition, and a weak temperature dependence in a liquid state. Right after the transition, that is temperatures above $kT = 0.0027$, the vertex fraction D stays close to a value of $X_D = 0.017$, while those for other types fluctuate around $X_G = 0.060$, $X_H = 0.035$, $X_I = 0.030$, and $X_L = 0.039$.

A few interesting results were obtained in Ref. [15], where the evolution of geometrical defects and vertex fractions in a laser-heated complex plasma was studied. It should be noted, though, that the goal of the study was to investigate solid superheating and not temperature dependencies of order parameters. The authors did not have a chance to vary the temperature of a system gradually as the heating source was turned on and off abruptly.

First, quadrilateral and pentagonal order parameters in a liquid state of the experimental system were found to be $P_4 \approx 0.19$ and $P_5 \approx 0.05$. These values fully agree with and support the results of our simulations. Second, the authors of Ref. [15] observed sudden spikes in the abundances of vertex types F and E at the times when the heating source was abruptly turned on and off. Whether it is a signature of vertex metastability or a specific temperature dependence remained unclear. In the view of our simulation results and, specifically Fig. 9, we conclude that the reason behind the spikes is an intrinsic temperature dependence of vertex fractions B, C, E, and F, with spikes corresponding to the temperatures lower than the final kinetic temperature of a liquid.

Just as in the case of the orientational parameters and topological defect fractions, an evolution of order parameters P and vertex fractions X during the gradual crystallization does not exactly duplicate the behavior throughout the heating phase. For example, a peak in the time dependence of the vertex fraction type E corresponds to the temperature of $kT \approx 0.0022$, as opposed to the temperature of $kT \approx 0.0025$ in the case of melting (Fig. 9). Critical values of X_B and X_C are also slightly shifted to lower temperatures. As the temperature is lowered further, the system crystallizes back to the nearly perfect hexagonal lattice, with only a few quadrilateral defects.

We have repeated our simulations starting with polycrystalline configurations, obtained from a rapidly cooled 2D Yukawa liquid. The evolution of order parameters throughout the initial heating phase turned out to be slightly configuration-dependent. For example, in a few cases orientational order parameters increased as the polycrystalline solid was heated, while at the same time topological defects diminished. This can be explained by the melting of grain boundaries and simultaneous merging of crystalline domains. Nevertheless, the point of a final transition to the liquid phase was found to be the same as in the case of the hexagonal initial configuration, that is, $kT \approx 0.0027$. Therefore, most of the results presented here would also hold for the melting of a polycrystalline solid.

IV. SUMMARY

In this paper we reported the results of Langevin dynamics simulations, performed to investigate two-dimensional melting and crystallization transitions in many particle Yukawa systems, such as those found in complex plasma experiments. To characterize the state of a system, we used the polygon construction method, in which unusually long bonds are deleted from the triangulation map of particle positions. Geometrical defects were identified as nontriangular polygons, while vertices were classified according to the type and order of polygons surrounding them. We also made use of a topological defect fraction and orientational order parameters as conventional tools to analyze phase transitions.

In our simulations of the system with the constant value of screening strength ($\kappa = 2$), the solid-to-liquid phase transition takes place in the coupling parameter range of $\Gamma \approx 400$–370, where rapid changes in order parameters and defect fractions were detected. The orientational and translational order is destroyed by the nonhomogeneous growth of large defect complexes and chains, contrary to the KTHNY theory of two-dimensional melting, which predicts the emergence of isolated dislocations and disclinations.

To quantify the disorder, we used polygonal order parameters P, that is, the normalized number of geometrical defects of a certain kind. It turned out that a liquid phase can be characterized by the temperature-independent value of a quadrilateral order parameter of $P_4 \approx 0.20$. In the context of pentagonal defects, the liquid state is characterized by the value of $P_5 > 0.03$. In our future work we plan to investigate the dependence of these characteristic values on the type of interaction potential.

Concentrations of vertices containing three or more quadrilaterals (D, G, H, and I) showed only a weak dependence on the temperature in the liquid state, showing the tendency for quadrilaterals to cluster together. Temperature dependencies of vertex fractions of the types B, C, E, and F all feature well expressed peaks at the beginning (E, F) or final stages (B, C) of the solid-liquid transition with a very similar behavior during the recrystallization. We suggest polygon construction method as a sensitive tool to characterize the state of a system and analyze two-dimensional phase transitions.

ACKNOWLEDGMENTS

The author thanks E. Anisimovas for valuable suggestions as well as two anonymous referees for helpful feedback.

[1] D. R. Nelson and B. I. Halperin, Phys. Rev. B **19**, 2457 (1979).
[2] A. P. Young, Phys. Rev. B **19**, 1855 (1979).
[3] V. Nosenko, S. K. Zhdanov, A. V. Ivlev, C. A. Knapek, and G. E. Morfill, Phys. Rev. Lett. **103**, 015001 (2009).
[4] S. T. Chui, Phys. Rev. Lett. **48**, 933 (1982).
[5] N. D. Mermin, Phys. Rev. **176**, 250 (1968).
[6] P. C. Hohenberg, Phys. Rev. **158**, 383 (1967).
[7] C. A. Knapek, D. Samsonov, S. Zhdanov, U. Konopka, and G. E. Morfill, Phys. Rev. Lett. **98**, 015004 (2007).
[8] C. A. Murray and D. H. Van Winkle, Phys. Rev. Lett. **58**, 1200 (1987).
[9] Z. Wang, A. M. Alsayed, A. G. Yodh, and Y. Han, J. Chem. Phys. **132**, 154501 (2010).
[10] V. M. Bedanov, G. V. Gadiyak, and Y. E. Lozovik, Phys. Lett. A **109**, 289 (1985).
[11] P. Hartmann, Z. Donkó, P. M. Bakshi, G. J. Kalman, and S. Kyrkos, IEEE Trans. Plasma Sci. **35**, 332 (2007).
[12] M. A. Glaser and N. A. Clark, Phys. Rev. A **41**, 4585 (1990).
[13] M. A. Glaser and N. A. Clark, Adv. Chem. Phys. **83**, 543 (1993).
[14] Y. Lansac, M. A. Glaser, and N. A. Clark, Phys. Rev. E **73**, 041501 (2006).
[15] W. D. Suranga Ruhunusiri, J. Goree, Yan Feng, and Bin Liu, Phys. Rev. E **83**, 066402 (2011).
[16] U. Konopka, G. E. Morfill, and L. Ratke, Phys. Rev. Lett. **84**, 891 (2000).
[17] G. E. Morfill and A. V. Ivlev, Rev. Mod. Phys. **81**, 1353 (2009).
[18] J. H. Chu and Lin I, Phys. Rev. Lett. **72**, 4009 (1994).
[19] H. Thomas, G. E. Morfill, V. Demmel, J. Goree, B. Feuerbacher, and D. Möhlmann, Phys. Rev. Lett. **73**, 652 (1994).
[20] Y. Feng, J. Goree, and B. Liu, Phys. Rev. Lett. **100**, 205007 (2008).
[21] G. J. Kalman, P. Hartmann, Z. Donkó, and M. Rosenberg, Phys. Rev. Lett. **92**, 065001 (2004).
[22] P. Hartmann, M. C. Sándor, A. Kovács, and Z. Donkó, Phys. Rev. E **84**, 016404 (2011).
[23] W. F. van Gunsteren and H. J. C. Berendsen, Mol. Phys. **45**, 637 (1982).
[24] R. D. Skeel and J. A. Izaguirre, Mol. Phys. **100**, 3885 (2002).
[25] A. Radzvilavicius and E. Anisimovas, J. Phys.: Condens. Matter **23**, 385301 (2011).
[26] Y. Feng, J. Goree, and B. Liu, Phys. Rev. Lett. **104**, 165003 (2010).
[27] H. M. Thomas and G. E. Morfill, Nature (London) **379**, 806 (1996).
[28] Y. Feng, B. Liu, and J. Goree, Phys. Rev. E **78**, 026415 (2008).
[29] J. D. Bernal, Nature (London) **185**, 68 (1960).
[30] K. J. Strandburg, Rev. Mod. Phys. **60**, 161 (1988).
[31] P. Hartmann, G. J. Kalman, Z. Donkó, and K. Kutasi, Phys. Rev. E **72**, 026409 (2005).
[32] I. V. Schweigert, V. A. Schweigert, and F. M. Peeters, Phys. Rev. B **60**, 14665 (1999).
[33] R. H. Morf, Phys. Rev. Lett. **43**, 931 (1979).
[34] R. A. Quinn and J. Goree, Phys. Rev. E **64**, 051404 (2001).
[35] W. K. Qi, S. M. Qin, X. Y. Zhao, and Y. Chen, J. Phys.: Condens. Matter **20**, 245102 (2008).